# Single photon induced symmetry breaking of $H_2$ dissociation

F. Martín[1], J. Fernández[1], T. Havermeier[2], L. Foucar[2], Th. Weber[2], K. Kreidi[2], M. Schöffler[2], L. Schmidt[2], T. Jahnke[2], O. Jagutzki[2], A. Czasch[2], E.P. Benis[4], T. Osipov[5], A. L. Landers[3], A. Belkacem[5], M. H. Prior[5], H. Schmidt-Böcking[2], C. L. Cocke[4], and R. Dörner[2]

[1] *Departamento de Química, C-9, Universidad Autónoma de Madrid, 28049-Madrid, Spain*

[2] *Institut für Kernphysik, University Frankfurt, Max von Laue Str 1, D-60438 Frankfurt Germany*

[3] *Department of Physics, Auburn University Auburn AL-36849*

[4] *Dept of Physics, Kansas State Univ, Cardwell Hall, Manhattan KS 66506*

[5] *Lawrence Berkeley National Lab., Berkeley CA 94720*

## Abstract

$H_2$, the smallest and most abundant molecule in the universe, has a perfectly symmetric ground state. What does it take to break this symmetry? Here we show that the inversion symmetry can be broken by absorption of a linearly polarized photon, which itself has inversion symmetry. In particular, the emission of a photoelectron with subsequent dissociation of the remaining $H_2^+$ fragment shows no symmetry with respect to the ionic $H^+$ and neutral H atomic fragments. This result is the consequence of the entanglement between symmetric and antisymmetric $H_2^+$ states resulting from autoionization. The mechanisms behind this symmetry breaking are general for all molecules.

Symmetries are essential building blocks of our physical, chemical and biological models. For macroscopic objects symmetries are always only approximate. By reducing the complexity in the microcosm these symmetries often become strict. Thus, in any symmetric molecule the ground state has a well defined parity. This property has far reaching consequences such as truncation of rotational spectra or the existence of ortho and para molecular isomers [1]. An intriguing way to break the symmetry is isotopic substitution of one of the nuclei [2]. In larger systems, symmetry breaking can also be achieved through selected vibrational modes, e.g., asymmetric stretch, which lies at the origin of the Jahn-Teller and Rener-Teller effects [3]. Alternatively, external fields can be used to favor a particular molecular direction, which has been recently used by Kling et al [4] to induce asymmetric dissociation of the $H_2^+$ molecular ion into a proton and a hydrogen atom. Here we show that, in dissociative ionization by absorption of a single photon (eq. 1)

$$h\nu + H_2 \rightarrow p + H + e^-, \tag{1}$$

symmetry breaking is possible even in the absence of an external field. This is the smallest and most fundamental molecular system for which such symmetry breaking is possible.

Symmetry operations in a molecule having a well-defined parity can change the sign of the ground state wave function (odd parity, or ungerade, states). However, all observables must be symmetric because they are squares of wave functions or transition matrix elements. To achieve left-right asymmetry in an observable, the system must be put into a coherent superposition of gerade (g, even), and ungerade (u, odd), molecular states. The relative phase between the two states can then lead to a left or right localization of an electron. Direct photoionization usually cannot induce this outcome, because the g and u states of the remaining molecular ion have different energies. Therefore, two ionization pathways are distinguishable by the electron energy and hence the coherence is lost.

Figure 1a shows the energy diagram for the $H_2$ and $H_2^+$ molecules. The energy difference between the lowest g and u states in $H_2^+$, $^2\Sigma_g^+(1s\sigma_g)$ and $^2\Sigma_u^+(2p\sigma_u)$ respectively, is about 17eV in the Franck Condon region of $H_2$. Thus if $H_2$ is directly ionized in a vertical transition by a photon of energy $h\nu$, the photoelectron will have an energy of about $E_e = h\nu - 16$eV when the remaining $H_2^+$ is left in the g state, whereas it will have $E_e = h\nu - 33$eV when it is left in the repulsive u state. Both ionization paths are distinguishable by the energy (fig. 1b and 1c). Because, in either path, $H_2^+$ is in a state of well defined parity, it manifests

no memory of the direction toward which the photoelectron is emitted. Here we show how such a memory becomes possible if indirect pathways of ionization via doubly excited states, such as those shown in figures 1d and 1e, are included in the picture.

The quantum dynamics of the population and decay of doubly excited states presents an important and fundamental challenge to theory. The full 4-body problem must be treated fully quantum mechanically without semiclassical approximations for the nuclear motion. We present an ab initio calculation that meets this challenge. In the accompanying kinematically complete experiment, we used the COLTRIMS technique [5, 6] to provide the most detailed possible check of this theory. We calculate and measure the vector momenta of the proton and the ejected electron in coincidence. Because the dissociation is rapid compared to molecular rotation, the direction of fragmentation coincides with the molecular orientation at the instant of electron emission. Thus measurements of the electron angular distribution afford data in the body fixed frame of the molecule, and asymmetry in the molecular dissociation can be observed with respect to the electron direction.

Doubly exited states and their decay give rise to the multitude of narrow structures, called Fano resonances [7], in atomic photoionization spectra. These oscillations in the cross section are the result of interference between two indistinguishable pathways through which the electron can be ejected. The photon can either expel an electron directly, or else promote the atom to a doubly excited state, which then decays after a delay by emission of one electron via autoionization. Because the final state in both of these pathways is the same, the amplitudes for each pathway must be added coherently, leading either to constructive or destructive interference, depending on the phase shift induced by the time delay. Doubly excited states have also been seen [8–11] and predicted ([12, 13] and references therein) for molecules. Because in molecules the excess photon energy can be distributed among internal nuclear and electron degrees of freedom however, the situation is much more complex than in atoms, and a clearcut proof of the interference effects is missing.

Here we clearly demonstrate such interference effects, and show that they cause symmetry breaking in dissociative photoionization. A first observation of asymmetric photoelectron emission from $H_2$ has been reported in pioneering experiments by Lafosse et al. [14]. In a different context, asymmetric electron emission has also been observed in $O_2$ [15] as the result of the decay of atomic oxygen following photodissociation of the $O_2$ molecule. In this case, the observed asymmetry thus does not strictly arise from a molecular decay process.

We used the framework of the dipole approximation given in Dill's formula [16] to evaluate photoionization cross sections corresponding to leaving the residual molecular ion in a specific electronic state $\alpha$, differential in $i$) the photoelectron energy $\epsilon$, $ii$) the photoelectron emission direction in the molecular frame $\Omega_e = (\theta_e, \phi_e)$ and $iii$) the polarization direction with respect to the molecular axis. The transition matrix element involves the ground molecular state of energy $W_{g\nu}$ and the final molecular state of energy $W_{\upsilon_\alpha} + \epsilon$ representing a molecular ion in the $\upsilon_\alpha$ vibronic state (either dissociative or non dissociative) and an emitted electron of energy $\epsilon$. Energy conservation dictates that $W_{g\nu} + h\nu = W_{\upsilon_\alpha} + \epsilon$. The two wave functions are connected by the dipole operator and are evaluated, neglecting rotational effects, in the adiabatic approximation using the theory of [17] (see also equations 42 and 60 of [18].)

Briefly, the final state comes from a close-coupling calculation incorporating contributions from the two lowest ionization thresholds of $H_2$, $[X^2\Sigma_g^+(1s\sigma_g)$, $^2\Sigma_u^+(2p\sigma_u)]$, the six lowest doubly excited states of the $Q_1$ and $Q_2$ series for both $\Sigma_u^+$ and $\Pi_u$ symmetries, as well as the corresponding vibrational and dissociative states. At variance with dissociative states associated with bound electronic states, those associated with doubly excited states are the solutions of a complex nonlocal differential equation that includes the possibility of autoionization decay as the molecule dissociates. Therefore, the final state wave function is not given simply by the product of an electronic and a nuclear wave function, but by a more complex form that accounts for interferences among the various electronic and nuclear channels. As shown in [18], the theory is formally exact within the adiabatic and nonrotation approximations provided that all electronic and nuclear differential equations are solved exactly.

Our computational methods used B-spline functions to obtain the electronic and vibrational wave functions, and are similar to those successfully applied to a variety of other dissociation-ionization problems in $H_2$ [13, 19, 20]. B-spline functions have also led, within the fixed-nuclear approximation, to the first numerical solution of the double photoionization of $H_2$ [21].

The experiments were performed at beamline 9.3.2 of the Advanced Light Source at Lawrence Berkeley National Laboratory. The monochromatized linearly polarized light from the synchrotron was crossed with an internally cold and localized supersonic $H_2$ and $D_2$ gas jet. The ions and electrons were directed by a combination of weak electric (20 V/cm) and parallel magnetic (10 Gauss) fields onto two position-sensitive microchannel plate detectors

with delayline position encoding [22]. Vector momenta were calculated from the position of impact and the times of flight of each particle. The energies of both ions and electrons were measured. Electron, ion and neutral fragment momenta $k_e, k_{p^+}$, and $k_H$ are related by momentum conservation: $k_e = -(k_{p^+} + k_H)$. Due to the light electron mass, the electron momentum is about 40 times smaller than the heavy particle momentum, leading to a nearly back-to-back fragmentation of proton and hydrogen atom. The energy deposited by the photon ($h\nu$) in excess of the threshold for dissociative ionization (eq. 1) of 18.6 eV is partitioned among the kinetic energy release (KER) of the heavy fragments, the electron energy ($E_e$) and internal excitation energy of the neutral ($h\nu = KER + E_e - 18.1eV - E_{exc}$). As expected, the hydrogen atom is found only in the ground state ($E_{exc} = 0$) in the photon energy range examined here. The asymptote of the $1s\sigma_g$ and $2p\sigma_u$ curve in figure 1 corresponds to a proton and a hydrogen atom in its ground state. Because both KER and $E_e$ are measured for each event, energy conservation can be used to very efficiently suppress random background or proton and electron pairs from residual water molecules in the chamber. The overall energy resolution is between 100meV and 0.5eV depending on the energy, the angular resolution about $5^o$. More detail on the COLTRIMS system can be found in [23].

For simplicity, we restrict the present discussion to an orientation of the molecule perpendicular to the polarization axis. This orientation selects transitions from the ground state of $\Sigma_g^+$ symmetry to excited states of $\Pi_u$ symmetry. Figure 2 shows the KER distribution for the reaction in eq. 1 as a function of the photon energy. Three areas with islands can be distinguished (I, II and III in Fig 2b): region I and III can be populated by direct ionization, leaving $H_2^+$ in the $2p\sigma_u$ or $1s\sigma_g$ state, respectively. However only the latter state contributes significantly, as a direct dipole transition from the $H_2$ ground state to the $2p\sigma_u k\pi_g$ continuum is very unlikely [13] (in fact, it would be strictly forbidden in an independent electron picture, $(1s\sigma_g)^2 \rightarrow 2p\sigma_u k\pi_g$). Thus regions I and II cannot be reached in a single-step direct photoionization. They are the fingerprint of a delayed emission of an Auger electron from $H_2$ doubly excited states (either $Q_1$ or $Q_2$). These states can either dissociate due to the repulsive character of the corresponding potential energy curve or decay by autoionization into the $2p\sigma_u$ or $1s\sigma_g$ states when such a decay is faster than the time required for an effective dissociation.

We distinguish 5 different pathways, all contributing to ionization in the photon energy

range of figure 2 and schematically shown in figures 1b, 1c, 1d and 1e (eq. 2-6

$$h\nu + \mathrm{H}_2 \rightarrow \mathrm{H}_2^+(1s\sigma_g) + e^- \ , \ \text{direct} \tag{2}$$

$$h\nu + \mathrm{H}_2 \rightarrow \mathrm{H}_2^+(2p\sigma_u) + e^- \ , \ \text{direct} \tag{3}$$

$$h\nu + \mathrm{H}_2 \rightarrow \mathrm{H}_2(\mathrm{Q}_1) \rightarrow \mathrm{H}_2^+(1s\sigma_g) + e^- \ , \ \text{resonant} \tag{4}$$

$$h\nu + \mathrm{H}_2 \rightarrow \mathrm{H}_2(\mathrm{Q}_2) \rightarrow \mathrm{H}_2^+(1s\sigma_g) + e^- \ , \ \text{resonant} \tag{5}$$

$$h\nu + \mathrm{H}_2 \rightarrow \mathrm{H}_2(\mathrm{Q}_2) \rightarrow \mathrm{H}_2^+(2p\sigma_u) + e^- \ , \ \text{resonant} \tag{6}$$

Asymptotically, $\mathrm{H}_2^+(2p\sigma_u)$ always leads to a dissociation, whereas $\mathrm{H}_2^+(1s\sigma_g)$ can lead either to $\mathrm{H}_2^+$ in a bound vibrational state or to a dissociative state. All these pathways must be added coherently if they yield the same electron energy and hence the same KER. Their interference leads to the distinct finger-like structures in the low KER region (fig. 2c-f). The calculated structures (fig. 2c,e) are in excellent agreement with the experimental observations (fig. 2d,f). Our calculations show that the structure is the result of an interference between the processes in eq. 2 and 4, the direct and resonant pathways leading to $1s\sigma_g$ in the same KER region. The finger-like structures are the molecular analogue of the well-known Fano interferences in the atomic case, but there are important differences entirely due to the molecular character of $\mathrm{H}_2$. As the photon energy increases, the position of a particular peak shifts to higher KER, which leads to fingers with a slope approximately equal to one. The number and position of the fingers is controlled by the overlap between the dissociative states associated respectively with processes in eqs. 2 and 4, so it is not surprising that the present experimental data and calculations for $\mathrm{H}_2$ and $\mathrm{D}_2$ show a large isotope effect on these structures (the different masses cause very distinct oscillations in the dissociative states).

We now turn to the angular distribution of the electron. We consider a photon energy of 33.25 eV and, as in the previous section, an orientation of the molecule perpendicular to the polarization axis. Figure 3 shows the key results of this work. Plotted is the angular distribution of the electron with respect to the polarization axis (horizontal). The plane of the figure is defined by the molecular axis and the polarization vector; only electrons in this plane are selected. The molecule is perpendicular to the polarization axis with the proton pointing upwards. The angular distributions are found to vary strongly with the kinetic energy release. Besides a change from a dumbbell to a butterfly shape, a strong asymmetry is found, in particular in a narrow range of KER $\simeq$ 8 to 10eV, corresponding to an electron

energy of $E_e \simeq 5$ to 7eV. All major features predicted by our theory are confirmed by the experimental data. They are also consistent with those reported in a previous experiment [14] by averaging over KER intervals of 2.5 to 3eV.

Our theoretical analysis allows us to distinguish the contributions leading to $1s\sigma_g$ (sum of processes in eqs. 2, 4 and 5) from those leading to $2p\sigma_u$ (sum of processes in eqs. 3 and 6). For a fixed photon energy of 33.25eV, the contributions of the $1s\sigma_g$ and $2p\sigma_u$ channels overlap in the 8 to 10eV region (fig. 4), where the largest asymmetry is observed (fig. 3).

How can the $1s\sigma_g$ and $2p\sigma_u$ channels interfere to produce an asymmetric angular distribution? To answer this question we have performed a model calculation in which we have only included the direct ionization channels, $1s\sigma_g k\pi_u$ and $2p\sigma_u k\pi_g$, and the lowest $Q_2$ state of $\Pi_u$ symmetry. The angular distributions found in this model calculation are very similar to those obtained from the full calculation (figure 3). In particular, the asymmetry is very well reproduced, showing that the $Q_1$ states are not responsible for its occurrence. We have then additionally excluded the two direct channels (eqs. 2 and 3) and only considered the decay of the $Q_2$ state through the channels in eqs. 5 and 6. The asymmetry remains, thus showing that the origin of the asymmetry is the interference between these two channels, i.e., between the resonant population of an ungerade and a gerade state. It is only the coherent superposition of these pathways which allows for a localization of the bound electron in the dissociating $H_2^+$. The transient molecule has broken symmetry and can keep a memory of the direction in which the electron departed. We have also found that the fingers in figure 2 do not appear when the direct channel (eq. 2) is not included in the calculation, thus confirming that their origin is the interference between resonant and non resonant population of the $1s\sigma_g$ state. In any case, the latter interference does not lead to a noticeable asymmetry.

The results of the full quantum calculation completely differ from those of the widely used simple semiclassical model (also used in fig. 1b-e for pedagogical purposes). In this simple model, the system always strictly follows the potential energy curves and only vertical transitions between them are allowed. These vertical transitions may occur as a result of photon absorption (vertical lines on the left) or autoionization decay (vertical lines on the right). In this framework all molecules have an identically well-defined value of the internuclear distance during the transition and, consequently, any possible direct energy exchange between electronic and nuclear motions is neglected. For example, in such a model the electron energy from the path shown by an orange line in fig. 1e (resonant

photoionization through the $2p\sigma_u$ channel) would be equal to the energy difference between the $Q_2$ and the $2p\sigma_u$ curve at the marked internuclear distance. Similar reasoning predicts the electron energy along the path shown by the green line (resonant photoionization through the $1s\sigma_g$ channel). Our calculations show that, in the present case, such simplified models, though of heuristic and pedagogical value, lead to false conclusions. The model predicts that the maximum possible value of the KER in the $1s\sigma_g$ channel is 8.1eV (corresponding to an autoionization decay at infinite internuclear distance), which is the minimum possible value of the KER in the $2p\sigma_u$ channel (corresponding to autoionization decay at the equilibrium internuclear distance). Therefore, no interference between g and u states can occur within this model because the electron energies and the KER regions for transitions to $1s\sigma_g$ and $2p\sigma_u$ would have no overlap, and hence the electron ejection would always be symmetric. Our fully quantum mechanical treatment shows that transitions to the $1s\sigma_g$ state can occur beyond 8.1eV and that transitions to the $2p\sigma_u$ state are possible even at zero KER. Thus the angular distribution can exhibit an asymmetry over the whole region of KER. Strictly speaking, a symmetric dissociation in the presence of resonances is the exception rather than the rule. It becomes quantitatively significant in the region where both channels are comparably active, between 8 and 10eV; however it is also visible in regions where one of the channels dominates (panels b-f in fig. 3).

It is worth noting that the observed asymmetry has no relation to the direction in which the charged fragment is emitted: sometimes the larger lobes are found on the proton side (panels c, d, and e), sometimes on the hydrogen side (panels b and f). Both theory and experiment show that the asymmetry oscillates with the KER, the amplitude of these oscillations being more important in the region where the $1s\sigma_g$ and $2p\sigma_u$ channels overlap. Between consecutive oscillations, there are KER values for which the distribution is practically symmetric. Thus the asymmetry cannot be explained by a preferred attractive interaction between the proton and the escaping electron (the latter is too fast to be efficiently perturbed by the slow proton, except possibly in the region of the maximum allowed KER).

Asymmetric photoelectron angular distributions should arise in any symmetric molecule that decays through two (or more) dissociative ionization channels associated with different symmetries of the residual molecular ion. When the final electron energy is the same in both channels, the corresponding ionization pathways are indistinguishable. This equivalence leads to interferences that depend on the time delay between the two ionization processes.

The time delay implies that the decay in either pathway occurs at different positions of the nuclei. This unique relationship between time delay and nuclear positions makes the problem of molecular autoionization much richer than the atomic case, with the asymmetry of the photoelectron angular distribution the most striking (and so far unexpected) effect. In conclusion, symmetry breaking should be considered a general molecular manifestation of autoionization when several decay channels are effectively accessible.

[1] I. N. Levine, *Molecular Spectroscopy* (John Wiley & Sons, Inc, 1975).

[2] D. Rolles *et al.*, *Nature* **437**, 711 (2005)

[3] G. Herzberg, *Molecular Spectra and Molecular Structure. Vol III. Electronic Spectra and Electronic Structure of Polyatomic Molecules* (Prentice-Hall, 1979).

[4] M. F. Kling *et al.*, *Science* **312**, 246 (2006)

[5] R. Dörner *et al.*, *Phys. Rep.* **330** 96 (2000).

[6] J. Ullrich *et al.*, *Rep. Prog. Phys.* **66** 1463 (2003).

[7] U. Fano, *Phys. Rev.* **124** 1866 (1961).

[8] S. Strathee and R. Browning, *J. Phys. B* **12** 1789 (1979).

[9] C. J. Latimer, J. Geddes, M. A. McDonald, N. Kouchi, and K. F. Dunn, *J. Phys. B* **29** 6113 (1996).

[10] K. Ito, R. I. Hall, and M. Ukai, *J. Chem. Phys.* **104**, 8449-8457 (1996).

[11] M. Lebech *et al.*, *Phys. Rev. Lett.* **96**, 173001 (2006).

[12] C. Bottcher and K. Docken, *J. Phys. B* **7**, L5 (1974).

[13] I. Sánchez, and F. Martín, *Phys. Rev. A* **60**, 2200 (1999).

[14] A. Lafosse *et al.*, *J. Phys. B* **36** 4683, (2003).

[15] A. V. Golovin *et al.*, *Phys. Rev. Lett.* **79** 4554 (1997).

[16] D. Dill, *J. Chem. Phys.* **65**, 1130 (1976).

[17] I. Sánchez and F. Martín, *Phys. Rev. Lett.* **82**, 3775 (1999).

[18] F. Martín, *J. Phys. B* **32**, R197 (1999).

[19] H. Bachau, E. Cormier, P. Decleva, J. E. Hansen, and F. Martín, *Rep. Prog. Phys.* **64**, 1815 (2001).

[20] G. Laurent *et al.*, *Phys. Rev. Lett.* **96** 173201 (2006).

[21] W. Vanroose, F. Martín, T. N. Rescigno, and C. W. McCurdy, *Science* **310**, 1787 (2005).

[22] O. Jagutzki *et al.*, *Nucl. Instr.Meth. A* bf 477 244 (2002)

[23] T. Jahnke *et al.*, *J. Elec. Spectr. Rel. Phen.* **141** 229 (2004)

[24] This work was supported in part by DGI project no. BFM2003-00194, the European COST action D26/0002/02, BMBF, DFG, DAAAD, the Division of Chemical Sciences, Geosciences and Biosciences Division, Office of Basic Energy Sciences, Office of Science, U. S. Department

of Energy and the Director, Office of Science, Office of Basic Energy Sciences and Division of Materials Sciences under U.S. Department of Energy Contract No. DE-AC03-76SF00098. We thank Roentdek GmbH (www.Roentdek.com) for support with the delayline detectors. We thank the "Centro de Computación Científica" of the UAM for its generous allocation of computer time. We are grateful for enlightening discussions with D. Dowek related to the effects observed in her group. We also acknowledge discussions with H.J. Lüdde. We are grateful for outstanding support by the staff at ALS in particular to B. S. Mun.

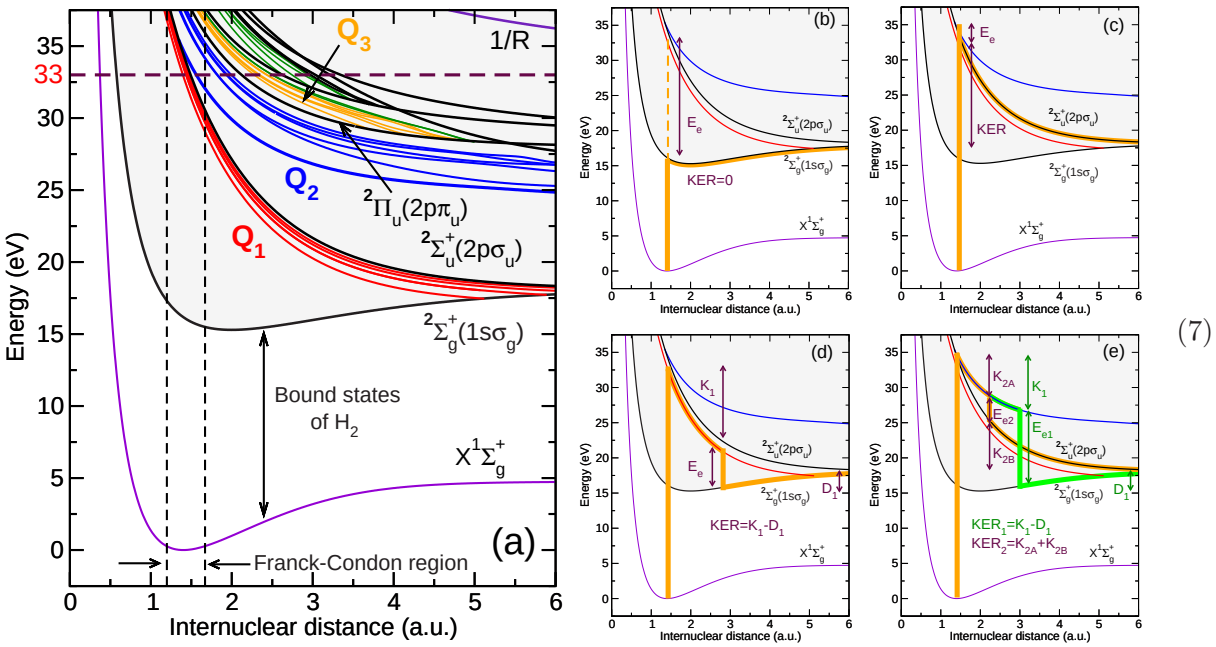


(7)

FIG. 1: Energy level diagram and pathways to dissociative ionization. (a) Total energy of the $H_2$ and $H_2^+$ systems as a function of internuclear distance. Red and blue are the lowest two series of doubly excited states of $H_2$ with $^1\Pi_u$ symmetry. At large internuclear distances the $Q_1$ states dissociate into $H(n=1)+H(n=2,...,\infty)$ and the $Q_2$ states into $H(n=2,l=1)+H(n=2,...,\infty)$, where $n$ and $l$ are the principle and angular momentum quantum numbers of the state. Panels (b), (c), (d), (e) show semiclassical pathways for dissociative ionization by absorption of one 33eV photon. (b) Direct ionization leading to $H_2^+(1s\sigma_g)$ (eq. 2 in the text). (c) Direct ionization leading to $H_2^+(2p\sigma_u)$ (eq. 3 in the text). (d) Resonant ionization through the lowest $Q_1$ doubly excited states leading to $H_2^+(1s\sigma_g)$ (eq. 4 in the text). (e) Resonant ionization through the lowest $Q_2$ doubly excited states leading to $H_2^+(1s\sigma_g)$ (eq. 5 in the text) or to $H_2^+(2p\sigma_u)$ (eq. 6 in the text).

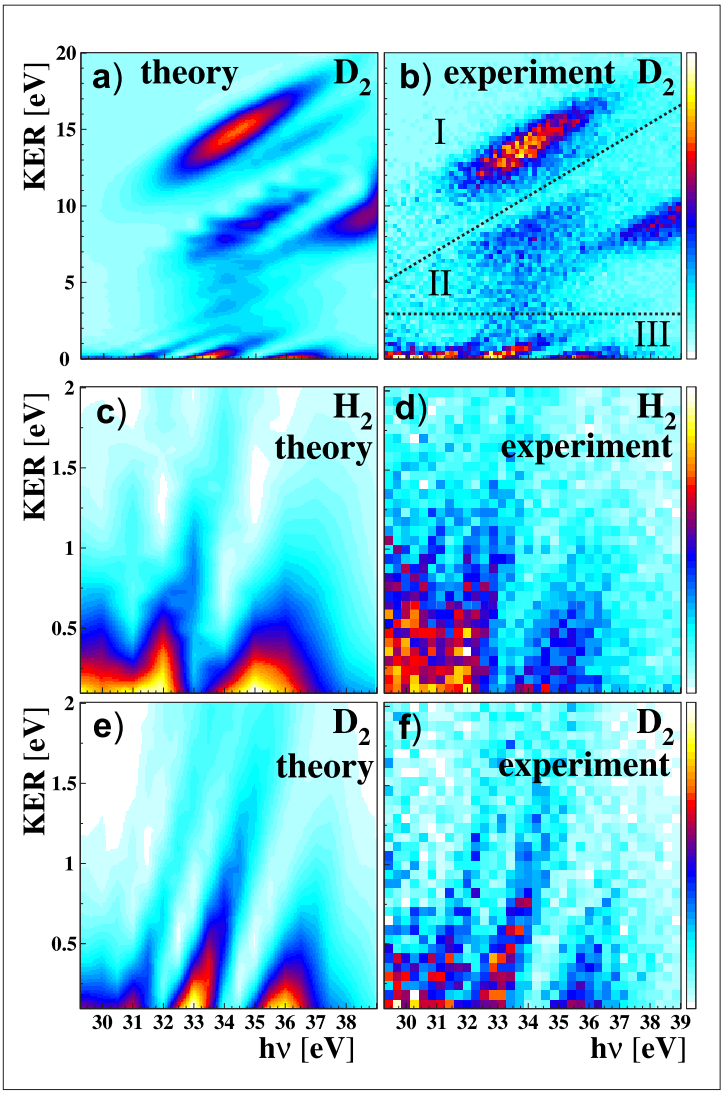


FIG. 2: Kinetic energy release as a function of photon energy for dissociative ionization of $H_2$ and $D_2$ (see eq. 1). (a) Theory and (b) experiment for $D_2$. For explanation of regions I, II and III, see text. (c)-(f) Magnification of the low KER region of panels (a) and (b) for $H_2$ (c and d) and $D_2$ (e and f). Left theory, right experiment.

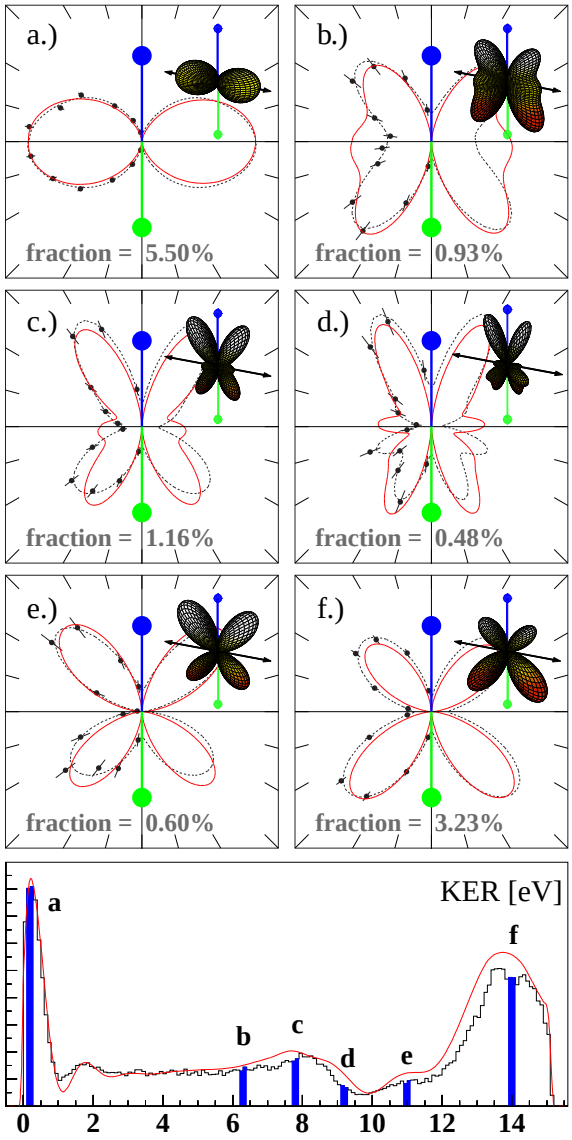


FIG. 3: Angular distribution of the electrons as a function of KER for dissociative ionization of $D_2$ (eq. 1) at a photon energy of 33.25eV, linearly polarized light. The angle-integrated KER spectrum is shown at the bottom (red line: theory, black line: experiment; letters a to f correspond to the six labelled spectra above; KER intervals: ±0.1eV). The orientation of the molecule at 90° to the polarization (theory) and 90±10° (experiment) is indicated by colored circles (blue = deuteron, green = deuterium). The (horizontal) polarization vector and the molecular axis define a common plane. The electron is restricted to this plane by ±45°. Full red line: theory, circles with error bars: experiment, dotted line: fit of the experimental data with spherical harmonics. The theoretical results have been integrated over the experimental acceptance angles and KER resolution as well as electron resolution. Infinite resolution theoretical results are shown by the small three-dimensional plots in the upper right; KER = 0.2 (a), 6.3 (b), 7.8 (c), 9.2 (d), 11 (e), and 14 eV (f).

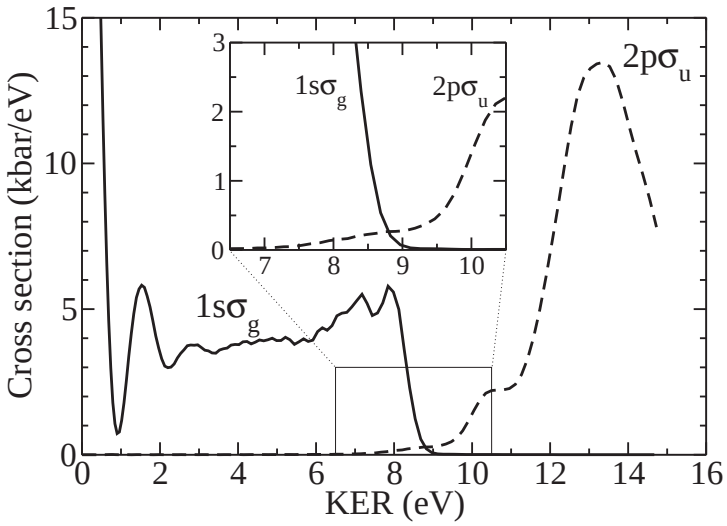


FIG. 4: Calculated $D^+$ kinetic energy distribution in dissociative ionization of $D_2$ by absorption of a 33.25eV photon. Full line: $1s\sigma_g$ channel. Dashed line: $2p\sigma_u$ channel. The inset is a blow-up of the squared region.